Nuclear Science and Techniques (2025) 36:195
https://doi.org/10.1007/s41365-025-01785-2

Searching for nuclei on the edge of stability with multi-step fragmentation

Xiu-Lin Wei[1] · Bao-Hua Sun[1] · Satoru Terashima[2] · Isao Tanihata[1] · Tian-Yu Wu[1] · Chang-Jian Wang[1]

Received: 26 March 2025 / Revised: 21 May 2025 / Accepted: 11 June 2025 / Published online: 5 August 2025

Abstract
Exploring the limits of neutron binding in atomic nuclei remains a central focus of nuclear physics. However, the experimental determination of the neutron drip line is challenging because of the minuscule production cross sections of the most neutron-rich isotopes. We investigate the effectiveness of multi-step fragmentation for producing extremely neutron-rich nuclides at relativistic energies. We demonstrate that multi-step fragmentation dominates over single-step fragmentation in thick-target experiments and can enhance the yields of drip-line nuclei by several orders of magnitude in a realistic experiment using fragment separators. Such enhancements open new possibilities for locating the drip lines above sodium and thus significantly expand the research horizon.

Keywords Multi-step fragmentation · Neutron drip line · Ion-optical simulation

1 Introduction

The number of naturally occurring nuclides on Earth is 339, including 256 stable nuclides and 83 radioactive nuclides. The possible number of bound nuclides has been predicted by nuclear models to be approximately 6000~9000 [1–3], for which only 3340 nuclides have been experimentally observed [4]. The nuclear drip line is the boundary beyond which the atomic nuclei are unbound to the emission of one or more proton(s) or neutron(s). Although the proton drip line has been extensively explored experimentally over the past decades, the neutron drip line has only been confirmed for light elements up to Ne [5].

The limit of nuclear existence is a fundamental subject in nuclear physics. Nuclei at or near drip lines can exhibit extreme structures [6], offering unique opportunities to study exotic open quantum behaviors and asymmetric nuclear matter. In addition to the naturally occurring radioactive nuclei, most unstable nuclei are artificially produced in accelerator facilities. Production methods are predominantly divided into two categories [7]: Isotope Separation On-Line (ISOL) and In-Flight (IF) fragment separation. ISOL facilities are renowned for generating high-purity isotopes with precise energies and low emittance, but suffer from poor extraction efficiencies for refractory materials and long extraction times for certain chemical elements. The In-Flight method effectively delivers all reaction products with lifetimes longer than several hundred ns, making it the most productive route for isotope discovery in recent years [8, 9]. Fission during flight, primarily involving actinide elements, is highly competitive for generating medium-mass neutron-rich nuclei (see Ref. [10]). Hybrid methods that integrate the strengths of ISOL and In-Flight techniques have attracted considerable interest because they offer promising opportunities to enhance the production yield of the most neutron-rich isotopes [11–13].

Despite significant progress in studying neutron-rich nuclei worldwide, exploring "terra incognita" near the neutron drip line remains challenging, where no data are

This work was partly supported by the National Natural Science Foundation of China (Nos. 12325506, 11961141004, 12335009, 12175009).

✉ Bao-Hua Sun
bhsun@buaa.edu.cn

Satoru Terashima
tera@impcas.ac.cn

[1] School of Physics, Beihang University, Beijing 100191, China

[2] Institute of Modern Physics, Chinese Academy of Sciences, Lanzhou 730000, China

available, primarily because of their small yield. In fragmentation reactions, the evaporation of neutrons from excited pre-fragments reduces the production cross sections of more neutron-rich nuclei [14, 15]. To address these challenges, numerous experimental strategies have been proposed to enhance beam intensity, spectrometer acceptance, and particle identification resolution at existing facility [16, 17]. However, they cannot fully compensate for the decreased production cross sections toward the neutron drip line.

There are various theoretical models from the empirical formula [18–20] to the hybrid method using Bayesian neural networks (BNNs) as well as Q_g systematics [21–23]. However, their extrapolations to systems with significant n/p asymmetry often exhibit large deviations. Transport models such as isospin-dependent quantum molecular dynamics [24] offer a microscopic description of the reaction mechanism and can reproduce experimental elemental fragmentation data fairly well [14, 25]. However, the QMD calculations are generally time-consuming and unsuitable for comprehensive calculations of multi-step fragmentation.

In this work, we investigate multi-step fragmentation reactions at relativistic energies of ~GeV/nucleon on a thick target to increase the yield of neutron-rich nuclei far from the stability line. In multi-step fragmentation, neutron-rich fragments can undergo further fragmentation processes, producing even more neutron-rich nuclei. This is due to the inherent "memory effect" in fragmentation reactions, which works efficiently to produce fragments with mass-to-charge ratios similar to those of neutron-rich projectile nuclei. Additionally, the diversity of intermediate nuclei increases the ejection probability of neutron-rich fragments to a certain extent [26–28].

In the present study, the effect of multi-step processes was illustrated using the drip line nucleus ^{34}Ne as an example. We simulated its production and transmission processes to evaluate the effectiveness and advantages of multi-step reactions. After optimizing the yields of neutron-rich nuclei, we estimated the production rates of neutron-rich nuclei above oxygen.

2 Production in the multi-step fragmentation

For a specific isotope of interest, the yield Y can be expressed as the product of three independent factors:

$$Y = \phi PS \tag{1}$$

where ϕ is the incident beam flux. P represents the probability of producing the nucleus of interest in the target, which depends on multiple factors such as nuclear interaction, beam energy, and target thickness. The third parameter S is the total transmission efficiency, which is determined by the momentum distribution of the fragments and acceptance of the detection system. Estimations of P and S for drip line nuclei were the main focus of the present study. To evaluate the factor P, one must consider not only the reactions of the projectile but also those of all the nuclei produced in the intermediate steps. Additionally, the angular and energy spreads of these product nuclei should be evaluated for the transmission factor S.

The production probability of the desired nuclide in a target, along with its angular and energy distribution, was calculated using the computer code LISE++ (version 16.18.20) [28, 29]. The fragment cross sections were calculated using the semi-empirical formula EPAX 2.15 [18], which has good precision in predicting the existing data near the neutron drip line in this mass region [30]. The slowing down processes, including energy loss, energy loss straggling, and angular straggling, were evaluated using the ATIMA 1.2 code [31, 32], with the results serving as input for subsequent calculations. The momentum distribution of the fragments was assessed based on Goldhaber theory [33]. A higher energy projectile is preferable to optimize the contribution of multi-step reactions; however, the accelerator facility imposes constraints on the energy choice. This study focuses on producing drip line nuclei near ^{34}Ne at the High-Intensity heavy-ion Accelerator Facility (HIAF) [17] under construction. Therefore, the projectile energy was set to 1500 MeV/nucleon.

The calculated production probability (P) of ^{34}Ne is shown in Fig. 1(a) as a function of target thickness for a ^{48}Ca beam incident on a Be target. The target thickness is expressed in units of the mean free path (λ), calculated using the reaction cross section of 1547 mb for ^{48}Ca on Be. In this case, the thickness λ corresponds to 9.68 g/cm^2 or 5.2 cm. As indicated in Fig. 1(a), the single-step production probability saturates at a thickness of approximately 1.03λ, which is significantly smaller than the thickness required for multi-step yields to plateau. Multi-step fragmentation dominates the production in thick targets, accounting for more than 95% of the total yield when the thickness exceeds λ. The corresponding peak value, observed at 3.33λ, was nearly 50 times higher than that obtained under the assumption of a single-step process alone. We also note that this optimized thickness holds for beam energies above 0.8 GeV/nucleon. However, as the target thickness increases, the effects of the incident particle attenuation and fragmentation of the objective nuclei become more pronounced, reducing the final production probability. Consequently, optimizing the target thickness is crucial to achieve a high yield of neutron-rich nuclei.

To determine which component plays a key role in multi-step fragmentation, we developed a dedicated code to compute the fragmentation yield, similar to Ref. [27].

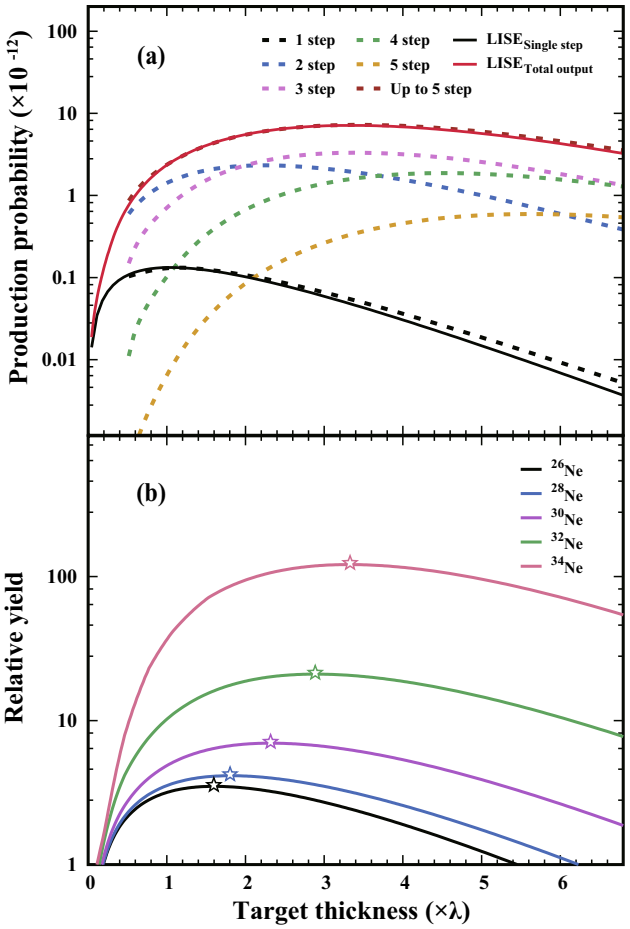

Fig. 1 (Color online) (a) Production probability of ^{34}Ne as a function of target thickness for the reaction of 1500 MeV/nucleon ^{48}Ca on Be. The single-step and multi-step processes are represented by black and colored lines, respectively. Solid and dashed lines distinguish the results from LISE++ and our code, respectively. (b) Same as Panel (a) but for the relative yields of Ne isotopes calculated using LISE++. The yields have been normalized to that at the 0.2λ thickness. The hollow pentagons indicate the peak positions

In this calculation, the reaction target was uniformly segmented along the beam direction. Each segment thickness is much smaller than the mean free path of projectile-like ions, so at most one reaction occurs per segment. The probability of fragment generation at each reaction point was calculated individually. The total probability was determined by evaluating all possible combinations of reaction positions and multi-step pathways. Figure 1(a) presents the calculated production probabilities from the single step to the fifth step. For target thicknesses of up to 2λ, the second-step reaction is the most crucial process. Above this thickness, the third-step process became predominant, steadily increasing its contribution. The contribution from the fifth step account for less than 4% of the total yield, while contributions beyond the fifth step are negligible. The inclusion of up to five steps in our simulation is sufficient for the absolute yield estimates and is well consistent with the LISE++ results.

We have computed the yields using other reaction models. Despite discrepancies in absolute values across models, the overall trends in the production probability of drip line fragments as a function of target thickness remained consistent, indicating that the enhancement via a multi-step mechanism in thick targets is a robust and model-independent feature.

To assess the yield of isotopes with varying neutron excesses, we present the relative yields of ^{26,28,30,32,34}Ne isotopes from the multi-step fragmentation in Fig. 1(b). A small scaling factor was introduced for the production probabilities to match the corresponding results at 0.6 GeV/nucleon. The yield curve for each isotope was normalized to the corresponding value at a thickness of 0.2λ. Although the curves exhibit a similar pattern across isotopes, the peak positions shift to a thicker thickness with increasing neutron excess. Two significant tendencies are observed: First, the yield enhancement at a larger λ is more pronounced for neutron-rich nuclei, indicating that multi-step fragmentation contributes more efficiently to their production. Second, the yield peaks at greater target thicknesses for more neutron-rich nuclei, highlighting the advantage of multi-step reactions in producing extremely neutron-rich nuclides. This pattern also holds for all neutron-rich isotopes. In contrast, increasing the target thickness to more than 1λ has little effect on the production of nuclei near the stability line. This pronounced disparity in yields suggests that employing a thick target for a relativistic projectile, where the multi-step fragmentation process gradually takes the lead, can compensate for the limitations associated with the smaller production cross sections of the most exotic nuclei. This approach has a clear advantage in pushing the limits of new isotope discovery.

3 Transmission of multi-step fragments

Reactions and penetration in a thick target inevitably lead to a notable increase in the beam transverse emittance and momentum spread, owing to the cumulative effects of fragmentation reactions and multiple scattering. Therefore, the fragments are eventually characterized by a high production rate but a broad momentum distribution. For experimental purposes, the separation, purification, and delivery of cocktail fragments to the terminal using a spectrometer or separator are often essential. The final yield at the experimental terminal is determined by the momentum distribution and the transmission efficiency of the spectrometer.

In the following, we take the HIgh-rigidity Radioactive Ion Beam Line (HIRIBL) of the HIAF facility (in construction) as a realistic case to illustrate the transmission of ejective fragments from a thick target. The HIRIBL, formerly known as the High-energy FRagment Separator (HFRS),

was designed to produce, separate, and purify rare isotopes with a maximum magnetic rigidity of 25 Tm. It is characterized by an angular acceptance of ±30 mrad (x) and ±15 mrad (y) and a momentum acceptance of ±2.0%. Details of the HIRIBL can be found in Refs. [34, 35]. The arrangement of the HIRIBL is shown in Fig. 2(a), with a Be production target at PF0. The reaction products were simulated at different focal planes. A clear particle identification is expected in the desired mass range.

The fragments are produced by bombarding a 1500 MeV/nucleon ^{48}Ca beam on Be, then transmitted and separated by HIRIBL. The beam intensity was 3×10^{11} particles per pulse (ppp). Each pulse lasted for 13 s. Acceptance calculations were performed using the Monte Carlo method implemented in LISE++. A high incident energy was beneficial for reducing the influence of the momentum distribution of the final product. Figure 2(b) illustrates the momentum distribution of ^{34}Ne fragments produced for various target thicknesses. A distinct asymmetric distribution is observed with a broad shoulder on the low-momentum side as the target thickness increases from 0.5λ to 3.0λ. The broadening is due to the energy loss difference between the projectile beam and the fragment. The distributions become symmetric after considering the momentum acceptance of the spectrometer for the optimized yield of ^{34}Ne.

Under the same target thicknesses, the momentum distributions at PF4 and MF6 exhibit similarity, with yields from PF4 to MF4 reduced by only 2.6% and 4.5% to MF6. In subsequent analyses, MF6 was used as the experimental terminal. Utilizing a thick target significantly reduces the transmission efficiency, as shown by the transmission efficiency curve in Fig. 2 (c). The transmission efficiency decreased from 92% at 0.21λ to 38% at 3.10λ. The impact of spectrometer acceptance on the final yield is also illustrated in Fig. 2 (c). The optimized target thickness with the HIRIBL transmission is slightly reduced from 3.33λ to 1.76λ, and the maximum yield decreases to 45% of the peak value obtained after the reaction target. However, using a thick target enhances the daily yield of ^{34}Ne by more than a factor of 30 compared with the case involving only single-step reactions. Moreover, utilizing a Ni projectile beam at the same beam intensity can enhance the ^{34}Ne yield rate by more than a factor of 130, as indicated in Fig. 3.

Finally, Fig. 3 summarizes the optimized production rates and the enhancement factor in producing the most neutron-rich isotopes between oxygen and chlorine using HIRIBL. The neutron drip lines predicted by the WS4 [1] and UNEDF1 [36] mass models are shown for comparison. The enhancement factor is the ratio between the production rates calculated using the multi-step fragmentation and those

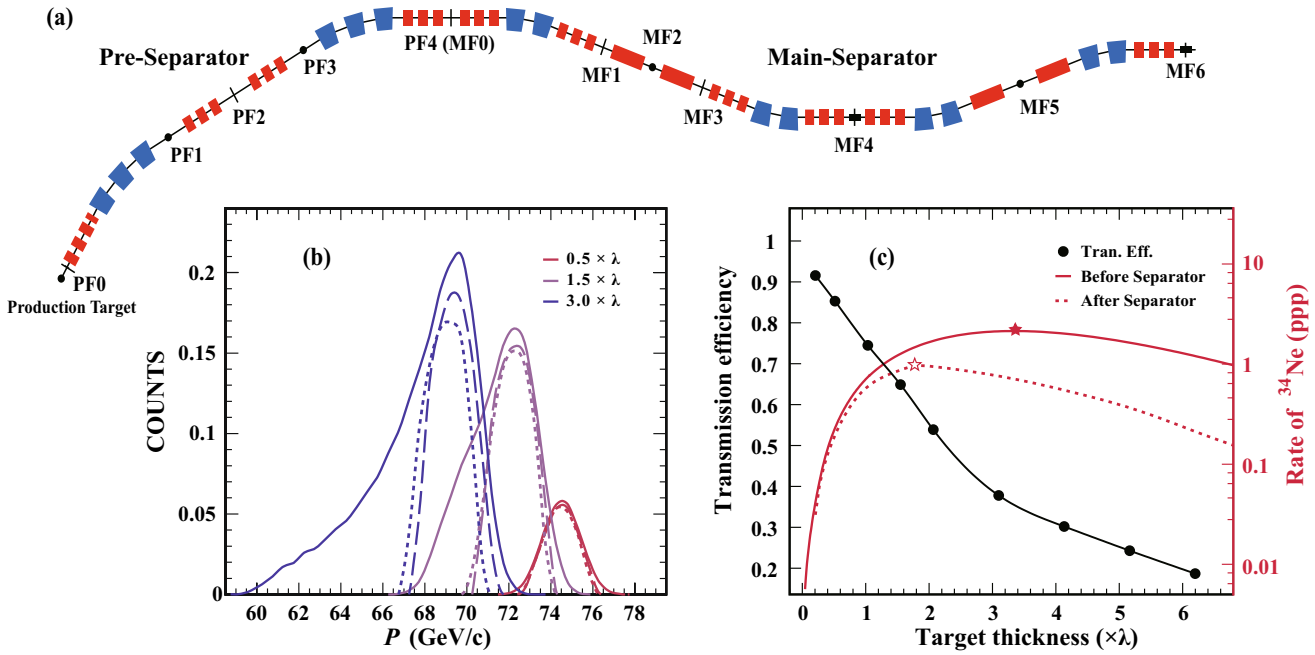

Fig. 2 (Color online) (a) Schematic layout of the HIRIBL. PF0-PF4 are the focal planes of the pre-separator, while MF0-MF6 correspond to the focal planes of the main separator. Dipole magnets are shown in blue, and multipole magnets in red. (b) Momentum distributions of ^{34}Ne expected after the reaction target at PF0 (solid lines), PF4 (dashed lines), and MF6 (dotted lines) for the target thicknesses of 0.5λ, 1.5λ, and 3.0λ. The projectile beam energy is fixed at 1500 MeV/nucleon with a beam intensity of 3×10^{11} ppp. (c) Production rate of ^{34}Ne (in particles per pulse) transmitted through HIRIBL as a function of target thickness. Solid and dashed lines represent results immediately after the target and at MF6 of HIRIBL, respectively, considering the multi-step fragmentation process. The black dots indicate the transmission efficiency at different target thicknesses

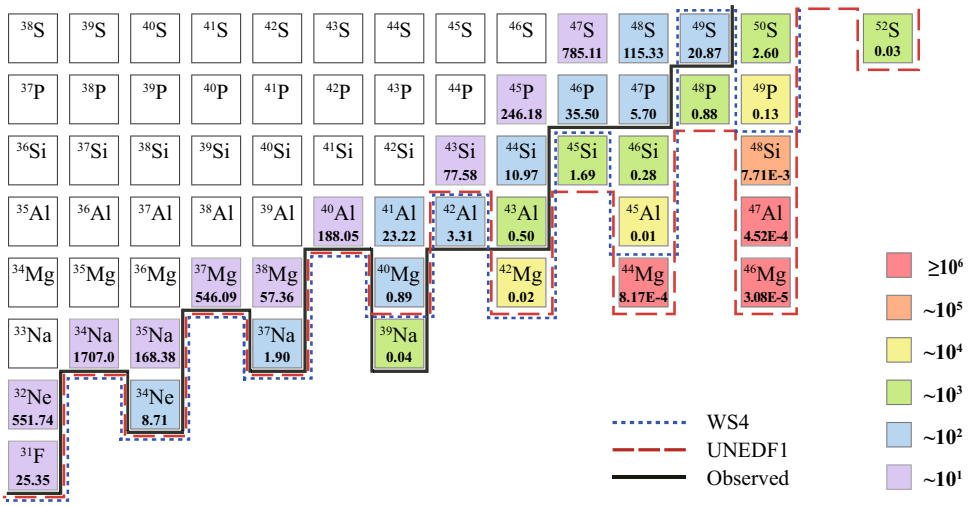

Fig. 3 (Color online) Estimated daily event rate of the most neutron-rich nuclei at HIRIBL, using the 1500 MeV/nucleon ^{64}Ni beam with an intensity of 3×10^{11} ppp on Be. The values in the square indicate the corresponding daily event rates. Color code represents the enhancement factors of the production rates for the multi-step fragmentation relative to those for the single-step process. The black line denotes the boundary of the observed nuclei experimentally. Nuclei to the right of the black line remain to be discovered. The neutron drip lines predicted by the WS4 [1] and UNEDF1 [36] mass models are shown by the blue dotted and red dashed lines, respectively

calculated using only the single-step process. The projectile beam of ^{64}Ni is assumed to be at 1500 MeV/nucleon and has an intensity of 3×10^{11} ppp. Each isotope was calculated to achieve the best production rate by optimizing the target thickness and transmission in the HIRIBL. Compared to single-step reactions alone, an increase of more than two orders of magnitude in the yields of the most exotic nuclei can typically be achieved. For example, the expected daily event rate of ^{45}Si increases from 1.28×10^{-3} to approximately 1.69. Other projectile nuclei such as ^{82}Se may help achieve even higher yields [37]. These enhancements provide new possibilities for locating the drip line above sodium and thus significantly expanding the research horizon.

4 Conclusion

In summary, the multi-step fragmentation of relativistic ions occurring in a thick target can significantly enhance the yields of neutron drip-line nuclei, effectively compensating for their low production cross section. This enhancement is a robust feature that is independent of the reaction model. The fragment separator HIRIBL is expected to be commissioned this year, and a proof-of-principle run will be planned during the first experimental run, which can be coupled naturally with charge-changing reaction studies [38–40]. When coupled with the fragment separator HIRIBL, the production rates can be boosted by several orders of magnitude. Employing a higher-acceptance separator will further highlight such improvements. Thus, the multi-step fragmentation processes open new avenues for searching for new isotopes at the edge of nuclear stability and exploring novel structures and phenomena in extremely neutron-rich nuclei.

Enhancing production rates is expected to be more effective at higher projectile energies, which will be available at HIAF and FAIR facilities. Although we have restricted the discussion to multi-step fragmentation, one can naturally extend the study to other combinations of reactions, such as projectile fission followed by multi-step fragmentation. Different combinations of multi-step processes can help increase specific isotope rates. We would also like to note that the effect of multi-step fragmentation is present at energies below GeV/nucleon, albeit with reduced efficacy.

Acknowledgements We are grateful to H.J. Ong and H. Suzuki for their helpful discussions.

Author contributions All authors contributed to the study conception and design. Material preparation, data collection and analysis were performed by Xiu-Lin Wei, Bao-Hua Sun, and Satoru Terashima. The first draft of the manuscript was written by Xiu-Lin Wei and Bao-Hua Sun, and all authors commented on previous versions of the manuscript. Isao Tanihata participated in the discussions and provided valuable suggestion during the preparation of the initial draft. All authors read and approved the final manuscript.

Data availability The data that support the findings of this study are openly available in Science Data Bank at https://cstr.cn/31253.11.sciencedb.j00186.00751 and https://www.doi.org/10.57760/sciencedb.j00186.00751.

Declarations

Conflict of interest The authors declare that they have no Conflict of interest.

References

1. N. Wang, M. Liu, X.Z. Wu et al., Surface diffuseness correction in global mass formula. Phys. Lett. B **734**, 215 (2014). https://doi.org/10.1016/j.physletb.2014.05.049
2. X.W. Xia, Y. Lim, P.W. Zhao et al., The limits of the nuclear landscape explored by the relativistic continuum Hartree-Bogoliubov theory. At. Data Nucl. Data Tables **121–122**, 1–215 (2018). https://doi.org/10.1016/j.adt.2017.09.001
3. L. Neufcourt, Y. Cao, S.A. Giuliani et al., Quantified limits of the nuclear landscape. Phys. Rev. C **101**, 044307 (2020). https://doi.org/10.1103/PhysRevC.101.044307
4. F.G. Kondev, M. Wang, W.J. Huang et al., The NUBASE2020 evaluation of nuclear physics properties. Chin. Phys. C **45**, 030001 (2021). https://doi.org/10.1088/1674-1137/abddae
5. D.S. Ahn, N. Fukuda, H. Geissel et al., Location of the Neutron Dripline at Fluorine and Neon. Phys. Rev. Lett. **123**, 212501 (2019). https://doi.org/10.1103/PhysRevLett.123.212501
6. Y.L. Ye, X.F. Yang, H. Sakurai et al., Physics of exotic nuclei. Nat. Rev. Phys. **7**, 21 (2025). https://doi.org/10.1038/s42254-024-00782-5
7. H. Geissel, G. Münzenberg, K. Riisager, Secondary exotic nuclear beams. Annu. Rev. Nucl. Part. Sci. **45**, 163 (1995). https://doi.org/10.1146/annurev.ns.45.120195.001115
8. C.W. Ma, H.L. Wei, X.Q. Liu et al., Nuclear fragments in projectile fragmentation reactions. Prog. Part. Nucl. Phys. **121**, 103911 (2021). https://doi.org/10.1016/j.ppnp.2021.103911
9. T. Nakamura, H. Sakurai, H. Watanabe, Exotic nuclei explored at in-flight separators. Prog. Part. Nucl. Phys. **97**, 53 (2017). https://doi.org/10.1016/j.ppnp.2017.05.001
10. N. Fukuda, T. Kubo, D. Kameda et al., Identification of new neutron-rich isotopes in the rare-earth region produced by 345 MeV/nucleon ^{238} U. J. Phys. Soc. Jpn. **97**, 014202 (2018). https://doi.org/10.7566/JPSJ.87.014202
11. D. Pérez-Loureiro, J. Benlliure, H. Álvarez-Pol et al., Production of neutron-rich nuclei in fragmentation reactions of ^{132}Sn projectiles at relativistic energies. Phys. Lett. B **703**, 552 (2011). https://doi.org/10.1016/j.physletb.2011.08.037
12. X.H. Sun, H. Wang, K. Yoneda et al., Production of neutron-rich nuclei in the vicinity of ^{78}Ni: Fragmentation reactions of unstable ^{81}Ga and ^{82}Ge beams. Phys. Lett. B **858**, 139081 (2024). https://doi.org/10.1016/j.physletb.2024.139081
13. B.Q. Cui, Y. Gao, Y.C. Ge et al., The Beijing ISOL initial conceptual design report. Nucl. Instrum. Meth. Phys. Res. B **317**, 257 (2013). https://doi.org/10.1016/j.nimb.2013.07.059
14. G.S. Li, B.H. Sun, J. Su et al., Single-proton removal reaction in the IQMD+GEMINI model benchmarked by elemental fragmentation cross sections of $^{29-33}$Si on carbon at ~230 MeV/nucleon. Phys. Lett. B **859**, 139143 (2024). https://doi.org/10.1016/j.physletb.2024.139143
15. J.W. Zhao, B.H. Sun, I. Tanihata et al., Isospin-dependence of the charge-changing cross-section shaped by the charged-particle evaporation process. Phys. Lett. B **847**, 138269 (2023). https://doi.org/10.1016/j.physletb.2023.138269
16. X.D. Xu, Y. Zheng, Z.Y. Sun et al., Full realization of the RIBLL2 separator at the HIRFL-CSR facility. Sci. Bull. **70**, 1026 (2025). https://doi.org/10.1016/j.scib.2025.01.020
17. X.H. Zhou, J.C. Yang, Status of the high-intensity heavy-ion accelerator facility in China. AAPPS Bull. **32**, 35 (2022). https://doi.org/10.1007/s43673-022-00064-1
18. K. Sümmerer, B. Blank, Modified empirical parametrization of fragmentation cross sections. Phys. Rev. C **61**, 034607 (2000). https://doi.org/10.1103/PhysRevC.61.034607
19. K. Sümmerer, Improved empirical parametrization of fragmentation cross sections. Phys. Rev. C **86**, 014601 (2012). https://doi.org/10.1103/PhysRevC.86.014601
20. B. Mei, Improved empirical parameterization for projectile fragmentation cross sections. Phys. Rev. C **95**, 034608 (2017). https://doi.org/10.1103/PhysRevC.95.034608
21. X.B. Wei, H.L. Wei, C.W. Ma et al., Predictions from several models for the cross sections of light neutron-rich isotopes by Q_g systematics in ^{40}Ar projectile-fragmentation reactions. Phys. Rev. C **111**, 034607 (2025). https://doi.org/10.1103/PhysRevC.111.034607
22. X.B. Wei, H.L. Wei, Y.T. Wang et al., Multiple-models predictions for drip line nuclides in projectile fragmentation of ^{40,48}Ca, ^{58,64}Ni, and ^{78,86}Kr at 140 MeV/u. Nucl. Sci. Tech. **33**, 155 (2022). https://doi.org/10.1007/s41365-022-01137-4
23. C.W. Ma, X.B. Wei, X.X. Chen et al., Precise machine learning models for fragment production in projectile fragmentation reactions using Bayesian neural networks. Chin. Phys. C **46**, 074104 (2022). https://doi.org/10.1088/1674-1137/ac5efb
24. J. Su, F.S. Zhang, B.A. Bian, Odd-even effect in heavy-ion collisions at intermediate energies Phys. Rev. C **83**, 014608 (2011). https://doi.org/10.1103/PhysRevC.83.014608
25. G.S. Li, J. Su, W.B.H. Sun et al., New measurement of the elemental fragmentation cross sections of 218 MeV/nucleon ^{28}Si on a carbon target. Phys. Rev. C **107**, 024609 (2023). https://doi.org/10.1103/PhysRevC.107.024609
26. C.L. Jiang, B.B. Back, I. Gomes et al., Yield calculations for a facility for short-lived nuclear beams. Nucl. Instrum. Meth. Phys. Res. A **492**, 57 (2002). https://doi.org/10.1016/S0168-9002(02)01352-9
27. A. Pawełkiewicz, Y. Charviakova, Z. Patyk et al., Secondary reactions in relativistic fragmentation of nuclei. Acta Phys. Pol. B **56**, 1-A3 (2025). https://doi.org/10.5506/APhysPolB.56.1-A3
28. D. Bazin, O. Tarasov, M. Lewitowicz et al., The program LISE: a simulation of fragment separators. Nucl. Instrum. Meth. Phys. Res. A **482**, 307 (2002). https://doi.org/10.1016/S0168-9002(01)01504-2
29. O.B. Tarasov, D. Bazin, LISE++: Radioactive beam production with in-flight separators. Nucl. Instrum. Meth. Phys. Res. B **266**, 4657 (2008). https://doi.org/10.1016/j.nimb.2008.05.110
30. H. Suzuki, T. Kubo, N. Fukuda et al., Production cross section measurements of radioactive isotopes by BigRIPS separator at RIKEN RI Beam Factory. Nucl. Instrum. Meth. Phys. Res. B **317**, 756 (2013). https://doi.org/10.1016/j.nimb.2013.08.049
31. H. Weick, A.H. Sørensen, H. Geissel et al., Energy-loss straggling of (200–1000) MeV/u uranium ions. Nucl. Instrum. Meth. Phys. Res. B **193**, 1–7 (2002). https://doi.org/10.1016/S0168-583X(02)00718-8
32. ATIMA web site, https://web-docs.gsi.de/weick/atima/. Accessed 24 Mar (2025)
33. A.S. Goldhaber, Statistical models of fragmentation processes. Phys. Lett. B **53**, 306 (1974). https://doi.org/10.1016/0370-2693(74)90388-8
34. L.N. Sheng, X.H. Zhang, J.Q. Zhang et al., Ion-optical design of high energy fragment separator (HFRS) at HIAF. Nucl. Instrum. Meth. Phys. Res. B **469**, 1–9 (2020). https://doi.org/10.1016/j.nimb.2020.02.026
35. L.N. Sheng, X.H. Zhang, H. Ren et al., Ion-optical updates and performance analysis of High energy FRagment Separator (HFRS) at HIAF. Nucl. Instrum. Meth. Phys. Res. B **547**, 165214 (2024). https://doi.org/10.1016/j.nimb.2023.165214
36. M. Kortelainen, J. McDonnell, W. Nazarewicz et al., Nuclear energy density optimization: Large deformations. Phys. Rev. C **85**, 024304 (2012). https://doi.org/10.1103/PhysRevC.85.024304
37. H. Suzuki, Determination of the neutron dripline at F and Ne and discovery of the heaviest Na isotope: ^{39}Na, Advances in

Radioactive Isotope Science, Avignon, France (2023). https://indico.in2p3.fr/event/19688/contributions/124319/
38. C.J. Wang, G. Guo, H.J. Ong et al., Charge-changing cross section measurements of 300 MeV/nucleon ^{28}Si on carbon and data analysis. Chin. Phys. C **47**, 084001 (2023). https://doi.org/10.1088/1674-1137/acd366
39. J.C. Zhang, B.H. Sun, I. Tanihata et al., A new approach for deducing rms proton radii from charge-changing reactions of neutron-rich nuclei and the reaction-target dependence. Sci. Bull. **69**, 1647 (2024). https://doi.org/10.1016/j.scib.2024.03.051
40. J.C Zhang, B.H. Sun, I. Tanihata et al., Charge pickup reaction cross section for neutron-rich p-shell isotopes at 900A MeV. Phys. Rev. X (2025) (Accepted). https://doi.org/10.1103/k9tj-jq8s